Dalton Transactions

PAPER

View Article Online
View Journal | View Issue

Cite this: *Dalton Trans.*, 2026, **55**, 2465

Dioxygen-promoted catalytic deformylation of aldehydes *via* hydrogen atom abstraction by $[Fe(TPP)]_2O$

Kai-Chun Hsu,[a,b,c] Bhakyaraj Kasi,[a,d,e] Tanmoy Pain[a] and Chen-Hsiung Hung *[a]

Hydrogen-atom abstraction (HAA) is a fundamental step in diverse oxidative transformations, typically mediated by high-valent metal–oxo species (M═O). However, direct demonstration of this process by μ-oxo-bridged iron(III) dimers remains scarce. Here, we demonstrate that the dimeric $[Fe(TPP)O]_2$ complex (TPP = tetraphenylporphyrin) inherently promotes HAA, with 2-phenylpropanal (2-PPA) as the substrate. Under aerobic conditions, the iron porphyrin dimer abstracts an α-carbon hydrogen atom to form a carbon-centered radical, as verified by EPR spin-trapping. A reaction of this radical with O_2 cleaves the C–C bond, affording acetophenone and a formyloxyl radical. Although the deformylation proceeds sluggishly at neutral pH (3% yield), adding triethylamine (Et_3N) regenerates the active dimer and boosts the yield to 97%. These results provide clear evidence for HAA by a μ-oxo iron(III) porphyrin dimer and underscore its promise for aerobic C–H and C–C bond activations when paired with a suitable base.

Received 25th October 2025,
Accepted 8th January 2026

DOI: 10.1039/d5dt02565f

rsc.li/dalton

Introduction

Hydrogen atom abstraction (HAA) is a fundamental step in oxidative catalysis, initiating C–H bond activation prior to subsequent coupling reactions or functional group transformation. It serves as a pivotal step in both biocatalytic processes and synthetic organic transformations.[1–5] In heme enzymes such as cytochrome P450s and peroxidases, high-valent iron(IV)-oxo intermediates mediate HAA *via* proton-coupled electron transfer (PCET), enabling selective hydroxylation reactions.[6–8] Inspired by these enzymatic systems, a wide range of synthetic iron porphyrinoid complexes or non-heme models have been developed as structural and functional mimics. Foundational studies by Grove and others[9–12] established a mechanistic model for ferryl species and the rebound pathway, which was later advanced through electronic-state tuning strategies introduced by Nam and coworkers.[13,14] These efforts have advanced mechanistic insights into C–H bond cleavage and oxygen-atom transfer by enabling precise control over the electronic and steric properties of the active species.[15–18]

In biomimetic studies employing iron porphyrins, μ-oxo-bridged iron(III) porphyrin dimers, such as $[Fe(TPP)]_2O$ (TPP = tetraphenylporphyrin), represent thermodynamically stable sink species that form from monomeric iron porphyrins under aerobic conditions.[19] Although the robust Fe–O–Fe core renders these dimers relatively inert under mild conditions, cleavage of the μ-oxo bridge under acidic or oxidative conditions generates monomeric species with enhanced oxidative potential, capable of engaging in HAA reactions.[20,21] While HAA reactivity is well established for mononuclear iron(IV)═O and iron(III)–OH species, the intrinsic reactivity and catalytic function of intact μ-oxo-bridged dinuclear iron porphyrin complexes remain comparatively underexplored.[22] Given that oxo- and hydroxo-bridged diiron centers play an active role in HAA processes and oxygen atom transfer in non-heme metalloenzymes,[23–26] this work seeks to address the fundamental questions surrounding the HAA reactivity of the μ-oxo-bridged porphyrinic dimer and to systematically probe their potential as biomimetic oxidants.

One particularly compelling application of HAA reactivity is the oxidative deformylation of aldehydes, a transformation relevant to both metabolic pathways and synthetic chemistry.[27] Aldehydes such as 2-phenylpropanal (2-PPA) can undergo C–C bond cleavage following the initial abstraction of the α-carbon hydrogen atom, generating radical or cationic intermediates.[28–31] Despite the importance of this reaction type, μ-oxo-bridged iron(III) porphyrins have rarely been explored as catalysts for aldehyde deformylation *via* HAA pathways. In this study, we investigate the reactivity of $[Fe(TPP)]_2O$

[a]*Institute of Chemistry, Academia Sinica, Nankang Taipei 115201, Taiwan. E-mail: chhung@gate.sinica.edu.tw*
[b]*Nano Science and Technology Program, Taiwan International Graduate Program, Academia Sinica, Taipei 115201, Taiwan*
[c]*Department of Chemistry, National Taiwan University, Taipei 106319, Taiwan*
[d]*Molecular Science and Technology Program, Taiwan International Graduate Program, Academia Sinica, Taipei 115201, Taiwan*
[e]*Department of Chemistry, National Tsing Hua University, Hsinchu 300044, Taiwan*

with 2-PPA to evaluate its potential as a hydrogen atom abstractor and catalyst for oxidative deformylation. This work seeks to elucidate new mechanistic possibilities for μ-oxo iron porphyrin dimers and expand their utility in oxidative C–H activations and C–C bond cleavages.

Results and discussion

Hydrogen atom abstraction promoted by $[Fe(TPP)]_2O$

The structural interconversion between $[Fe^{III}(TPP)Cl]$ (**1**) and the μ-oxo-bridged dimer $[Fe^{III}(TPP)]_2O$ (**2**) occurs *via* a reversible acid–base reaction, as illustrated in Scheme 1 (Fig. S1–S7).[32] In the presence of a weak base such as triethylamine (Et_3N), two equivalents of the monomeric complex **1** and one equivalent of water generate the oxo-bridged dimer **2**. Conversely, treatment of **2** with a Brønsted acid (*e.g.*, HCl) regenerates the monomeric species **1**. The dimeric complex **2** contains a bridging oxo ligand connecting two high-valent iron(III) centers and is generally regarded as a thermodynamically stable resting state in porphyrin chemistry. Although it is less reactive in HAA than high-valent terminal Fe(IV)=O porphyrin species, its electronic structure suggests that it may participate in PCET pathways.

Previous studies have shown that the bond dissociation free energies (BDFEs) for hydrogen abstraction of the keto and enol forms of 2-phenylpropanal (2-PPA) are relatively low—66.1 and 55.9 kcal mol^{-1}, respectively—rendering them susceptible to HAA activation.[33] In this context, oxidative deformylation of 2-PPA *via* a HAA pathway leads to C–C bond cleavage following reaction with dioxygen, producing acetophenone and formic acid as the major products (Scheme 2).

The HAA reactivity of $[Fe^{III}(TPP)Cl]$ (**1**) and $[Fe^{III}(TPP)]_2O$ (**2**) was investigated using 2-PPA as a substrate, with product formation monitored by UV-Vis and ^1H NMR spectroscopy. CH_2Cl_2 solutions of **1** or **2** were treated with excess 2-PPA (100 equiv. for ^1H NMR and 2000 equiv. for UV-Vis measurements) under either aerobic or anaerobic conditions. Under aerobic

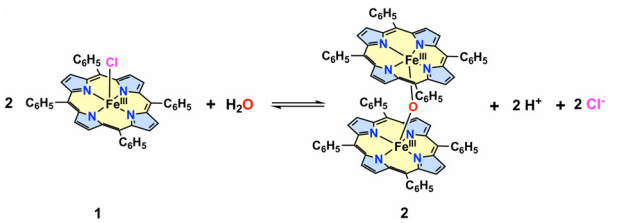

Scheme 1 Transformation between the Fe(III) monomer and μ-oxo-bridged dimer.

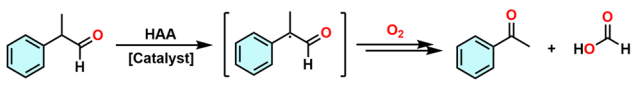

Scheme 2 Oxidative deformylation reaction of 2-PPA.

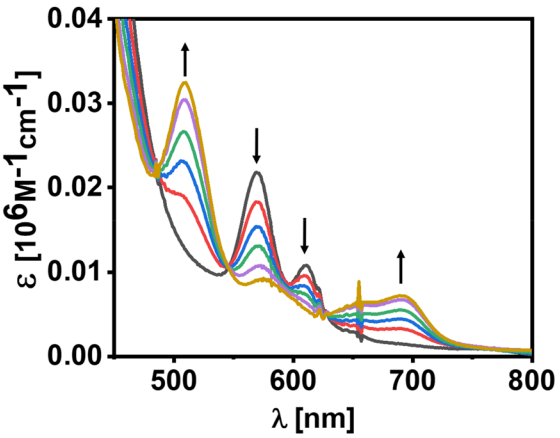

Fig. 1 UV-Vis spectrum of **2** in the presence of oxygen upon addition of 2-PPA in CH_2Cl_2.

conditions, the UV-Vis spectrum of **2** showed a decrease in the characteristic Q-bands at 570 and 612 nm, accompanied by an increase in absorption at 508 and 692 nm, indicating the formation of monomeric iron(III) species (Fig. 1). Concurrently, ^1H NMR analysis confirmed the conversion of 2-PPA into acetophenone with diagnostic resonances at 7.96, 2.58 ppm, consistent with oxidative deformylation (Fig. S8). By contrast, solutions of **1** showed no detectable spectral change under aerobic conditions. Under anaerobic conditions, no significant changes were observed in the UV–vis spectra of either **1** or **2** upon addition of 2-PPA, and no products were detected by ^1H NMR, even in the presence of a large excess of 2-PPA. These results suggest that molecular oxygen is essential for driving the reaction and that the HAA step is mediated by **2** in the oxidative deformylation of 2-PPA.

To investigate the nature of the monomeric iron(III) species generated from the reaction, formic acid (HCOOH) was introduced into a solution of complex **2**. The addition of only 1 μL of HCOOH induced an immediate change in the UV-Vis spectrum. The characteristic Q-bands of **2** at 570 and 612 nm decreased markedly, while new absorption features emerged at 508 and 692 nm. These spectral changes are consistent with the formation of a monomeric iron(III) species, tentatively assigned as $[Fe^{III}(TPP)(HCOO)]$, in which the formate anion coordinates as an axial ligand (Fig. S9). The proposed $[Fe^{III}(TPP)(HCOO)]$ species was further confirmed by ESI-MS analysis (Fig. S10).

Kinetic study

Kinetic measurements were performed to evaluate the HAA reactivity of **2** by time-dependent UV-Vis spectroscopy, varying the concentration of 2-PPA (10, 20, 30, 40, and 50 mM) while maintaining a fixed concentration of **2** (5 μM) under an O_2 atmosphere. No spectral changes were observed prior to O_2 addition, confirming that the reaction commenced only after O_2 was added. Under these conditions, the concentrations of 2-PPA and O_2 remained effectively constant, allowing the

observed spectral changes of **2** to be analyzed under pseudo-first-order conditions. Kinetic analysis of the absorbance decay at 570 nm yielded pseudo-first-order rate constants (k_{obs}) associated with the conversion of **2** to monomer iron(III) species. A linear dependence of k_{obs} on [2-PPA] was observed, affording a second-order rate constant (k_2) of 1.41×10^{-2} M^{-1} s^{-1} (Fig. 2). The approximately linear dependence on [2-PPA] indicates that the rate-determining step under these conditions involves **2** and the substrate.

Importantly, determination of this second-order rate constant provides a quantitative measure of the intrinsic HAA reactivity of the μ-oxo dimer. In comparison, high-valent iron (IV)-oxo species reported in the literature exhibit second-order rate constants on the order of 10^2–10^7 M^{-1} s^{-1} toward benzylic C–H or O–H bonds.[34–36] Accordingly, the measured k_2 value for **2** (1.41×10^{-2} M^{-1} s^{-1}) is several orders of magnitude lower. This comparison implies that while **2** is capable of abstracting hydrogen atoms from 2-PPA, its intrinsic reactivity is much less than that of high-valent iron(IV)-oxo species. Furthermore, the absence of detectable reactivity for the monomeric complex **1** under identical aerobic conditions indicates that the reaction is unlikely to proceed *via* an *in situ*-generated Fe(IV)=O intermediate, as such a species would also be expected to be accessible from the monomer. Consistent with this conclusion, the spectral evolution exhibited a well-defined isosbestic point, indicative of a clean conversion of the dimer to the monomer without accumulation of additional intermediates. Collectively, these observations support **2** as the active species responsible for HAA and the subsequent oxidative deformylation of 2-PPA.

EPR study revealing the intermediates of 2-PPA oxidative deformylation

To provide direct evidence for the proposed HAA mechanism, the formation of a 2-PPA-derived radical intermediate was confirmed using the spin-trapping reagent 5,5-dimethyl-1-pyrroline *N*-oxide (DMPO). DMPO is a well-established spin trap that forms stable adducts with a wide range of radical species —including O-, C-, N-, and S-centered radicals—yielding characteristic electron paramagnetic resonance (EPR) signals defined by distinct hyperfine coupling constants (a_N and a_H^β). In this system, hydrogen atom abstraction from the α-position (C_α) of 2-PPA produces a carbon-centered radical intermediate (PhCH·CH=O). A CH_2Cl_2 solution containing complex **2**, 2-PPA, and excess DMPO was prepared and analyzed by EPR spectroscopy under an inert atmosphere at 25 °C.

As shown in Fig. 3, the EPR spectrum displayed a complex signal pattern that could be deconvoluted into two sets of signals, each corresponding to a distinct DMPO–radical adduct. Both exhibited an identical *g*-value of 2.0012, consistent with carbon-centered radical species. The hyperfine coupling constants were determined as follows: conformer **1** (70% population) with a_N = 14.194 G and a_H^β = 22.522 G and conformer **2** (30% population) with a_N = 14.428 G and a_H^β = 19.370 G. These two species arise because radical trapping by DMPO creates two stereocenters (Fig. S11, at the α-carbon of 2-PPA and at the C2 carbon of DMPO), leading to two diastereomeric pairs of adducts (RR/SS and RS/SR). Each pair exists as a racemic mixture of enantiomers, which are indistinguishable by EPR; however, the two diastereomeric pairs exhibit distinct hyperfine parameters and unequal populations.[37] Conformer **1** corresponds to the major diastereomer and is likely stabilized by reduced steric repulsion between the phenyl/formyl substituents and the DMPO ring, as well as electronic factors that favor radical stabilization. Altogether with EPR detection of a substrate-derived radical and product analysis, these findings strongly support the assignment of **2** as the species directly engaged in hydrogen atom abstraction and oxidative aldehyde deformylation.

Proposed mechanism

A plausible mechanism for the deformylation of 2-PPA is presented in Scheme 3. In the initial step, $[Fe^{III}(TPP)]_2O$ (**2**) abstracts a hydrogen atom from the α-position of 2-PPA. This

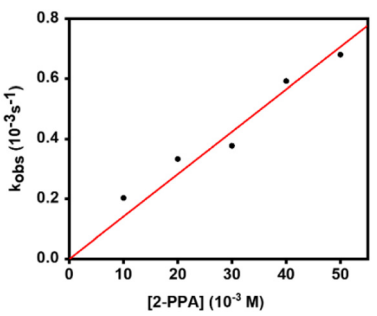

Fig. 2 Kinetics of the reaction of **2** with excess 2-PPA.

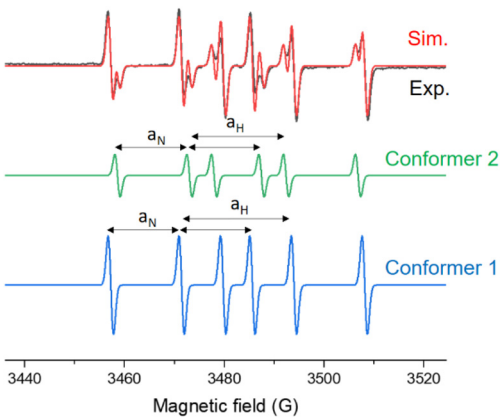

Fig. 3 X-Band CW-EPR spectrum (black) and spectral simulations of conformer 1 (blue), conformer 2 (green) and their combined fit (red). The spectrum was recorded at room temperature for a reaction mixture containing **2** (3 μmol), 2-PPA (0.30 mmol), and DMPO (0.04 mmol) in CH_2Cl_2 (1.0 mL) under an inert atmosphere. Instrument settings: microwave power 20 mW; modulation frequency 100 kHz; modulation amplitude, 1 G. The best-fit simulation (red) indicates two sets of signals with identical g = 2.0012 but distinct hyperfine coupling constants, as detailed in the text.

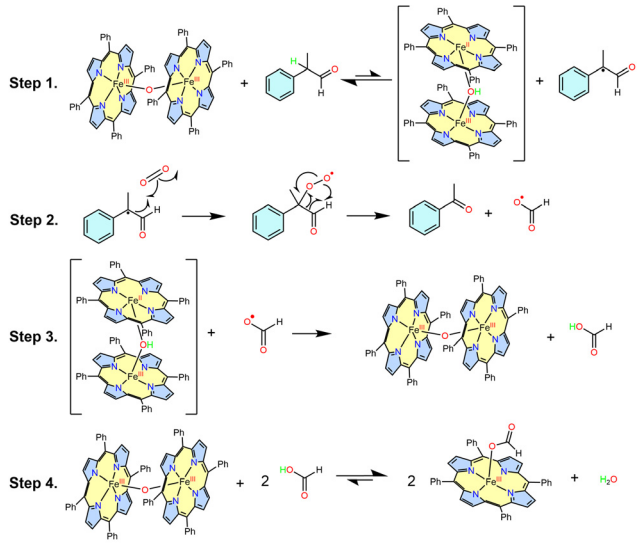

Scheme 3 Proposed mechanism of hydrogen atom abstraction.

involves proton transfer to the bridging oxo ligand and electron transfer to one of the Fe^{III} centers, yielding a 2-PPA radical and a mixed-valence intermediate, [(TPP)Fe^{II}–OH–Fe^{III}(TPP)] (Step 1). This HAA step is reversible, and under anaerobic conditions the equilibrium favors the starting materials, resulting in no observable spectral changes for **2**. Upon exposure to dioxygen, the 2-PPA-derived radical reacts with O_2 to form a peroxyhemiacetal intermediate, which facilitates C–C bond cleavage between the α-carbon and the carbonyl carbon, yielding acetophenone and a formyloxyl radical (Step 2). The latter can subsequently accept a proton and an electron from the mixed-valence intermediate, regenerating the μ-oxo dimer and producing formic acid (Step 3). As formic acid accumulates, the increasing acidic environment destabilizes **2**, promoting its conversion to the monomeric species [Fe^{III}(TPP)($HCOO^-$)] (Step 4). Collectively, these steps underscore the essential role of dioxygen in shifting the reaction equilibrium and enabling irreversible progression of the oxidative deformylation pathway.

The accumulation of formic acid converts **2** into the formate-bound species [Fe^{III}(TPP)(HCOO)], thereby suppressing its HAA reactivity. In an attempt to regenerate **2**, triethylamine (Et_3N) was added as a base after formation of [Fe^{III}(TPP)(HCOO)]. However, addition of Et_3N at this stage resulted in rapid spectral degradation, characterized by attenuation of the Soret and Q bands, indicative of decomposition of the porphyrin complex (Fig. S12).

The μ-oxo diiron tetraphenylporphyrin dimer, **2**, is best understood as a redox mediator and operative resting state in this catalytic system. One-electron reductions of [(TPP)Fe]$_2$O have been definitively characterized by Kadish and co-workers using *in situ* ESR spectroelectrochemistry, confirming the accessibility of mixed-valence μ-oxo Fe(II)/Fe(III) states.[38] Although reduced μ-hydroxo Fe(II)/Fe(III) dimers are rarely isolated crystallographically due to their high reactivity and rapid proton-coupled reorganization, their transient formation immediately following hydrogen-atom abstraction is kinetically reasonable. Under our aerobic basic conditions, any reduced μ-hydroxo Fe(II)/Fe(III) dimer generated in Step 1 would be rapidly intercepted by proton-coupled electron transfer from the highly reactive formyloxyl radical (˙OCHO) formed after C–C cleavage, thereby regenerating the stable μ-oxo mediator without accumulating to detectable concentration.

Catalytic 2-PPA oxidative deformylation under basic conditions

To examine the feasibility of establishing a catalytic cycle, two control experiments were performed (Fig. S13). First, preformed formate (generated by neutralization of formic acid with Et_3N) was added to a solution of **2**. Second, 2-PPA was added to a solution of **2** in the presence of Et_3N. In both cases, no significant UV-Vis spectral changes associated with **2** were observed, indicating that **2** remains stable under basic conditions and retains the potential to function as a catalyst. On this basis, the catalytic oxidative deformylation of 2-phenylpropanal (2-PPA) by [Fe(TPP)]$_2$O (**2**) was systematically investigated under varying stoichiometries, with or without Et_3N as an additive.

All reactions were performed in CH_2Cl_2 under the conditions outlined in Scheme 4 and summarized in Table 1. Under a nitrogen atmosphere, no formation of acetophenone

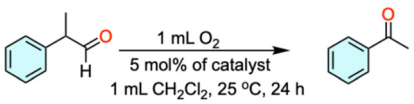

Scheme 4 Catalytic 2-PPA deformylation.

Table 1 Catalytic oxidative deformylation of 2-PPA using iron(III) porphyrin complex **1** or **2** under various conditions

Entry	Catalyst	Additive	Oxidant	Yield (%)	TON
1[a]	Fe^{III}(TPP)Cl	Et_3N	—	0	0
2[a]	[Fe^{III}(TPP)]$_2$O	Et_3N	—	0	0
3[a]	Fe^{III}(TPP)Cl	—	O_2	0	0
4[a]	[Fe^{III}(TPP)]$_2$O	—	O_2	3	0.6
5[a]	—	Et_3N	O_2	0	0
6[a]	Fe^{III}(TPP)Cl	Et_3N	O_2	97	19.4
7[a]	[Fe^{III}(TPP)]$_2$O	Et_3N	O_2	97	19.4
8[b]	Fe^{III}(TPP)Cl	Et_3N	O_2	36	36
9[b]	[Fe^{III}(TPP)]$_2$O	Et_3N	O_2	37	37
10[c]	Fe^{III}(TPP)Cl	Et_3N	O_2	84	84
11[c]	[Fe^{III}(TPP)]$_2$O	Et_3N	O_2	75	75
12[c]	Fe^{III}(acac)$_3$	Et_3N	O_2	22	22
13[c]	$FcPF_6$	Et_3N	O_2	8	8
14[c]	$Fe^{III}Cl_3$	Et_3N	O_2	5	5

Reaction conditions (general): 2-PPA (3×10^{-2} mmol), O_2 (1 mL), CH_2Cl_2 (1 mL); stirred at 25 °C. [a] Et_3N (3×10^{-2} mmol), catalyst **1** (3×10^{-3} mmol) or **2** (1.5×10^{-3} mmol); reaction time 24 h. [b] Et_3N (6×10^{-3} mmol), catalyst **1** (6×10^{-4} mmol) or **2** (3×10^{-4} mmol); reaction time 12 h. [c] Et_3N (3×10^{-2} mmol), catalyst **2** (3×10^{-4} mmol) or **1**/other iron salts (6×10^{-4} mmol); reaction time 20 h.

was observed with either [Fe^{III}(TPP)Cl] (**1**) or dimeric **2**, confirming the essential role of molecular oxygen in the transformation (entries 1 and 2). Under aerobic conditions but in the absence of Et_3N, monomeric complex **1** showed no catalytic activity, while **2** afforded only 3% acetophenone, corresponding to a ~60% yield based on a single stoichiometric turnover. These results indicate that the reaction does not proceed catalytically under neutral conditions (entries 3 and 4).

Remarkably, the addition of Et_3N under aerobic conditions led to a substantial enhancement in reactivity. In the presence of either **1** or **2**, the yield of acetophenone increased to 97%, indicative of highly efficient catalysis (entries 5–7). Notably, the catalytic activities of **1** and **2** were essentially identical. This behavior is consistent with rapid *in situ* conversion of the monomeric iron(III) porphyrin (**1**) into the μ-oxo-bridged dimer (**2**) under basic aerobic conditions, suggesting that both species operate through a common mechanism involving the oxo-dimer intermediate.

To further assess whether a significant difference exists between catalysts **1** and **2** under catalytic conditions, the substrate loading was increased to 100 equivalents (entries 8 and 9), and the reactions were monitored by gas chromatography. After 12 h, comparable yields were observed for catalyst **1** (36%) and catalyst **2** (37%), indicating no discernible difference in the catalytic performance over this time frame (Fig. S14). When the amount of Et_3N was further increased to 100 equivalents (entries 10 and 11), the reaction yields after 20 hours increased markedly to 84% and 75% for catalysts **1** and **2**, respectively, corresponding to a maximum turnover number of 84 (Fig. S15). The enhanced performance observed at high Et_3N loading is attributed to more efficient proton scavenging, which stabilizes the active μ-oxo-dimer **2** and facilitates sustained catalytic turnover.

For comparison, iron(III) acetylacetonate ($Fe(acac)_3$), ferrocenium hexafluorophosphate ($FcPF_6$), and iron(III) chloride ($FeCl_3$) were also evaluated as catalysts under otherwise identical basic conditions (entries 12–14). In contrast to **1** and **2**, these iron salts exhibited only minimal reactivity. This behavior likely reflects fundamentally different proton-coupled electron (PCET) pathways available to a simple Fe(III) oxidant in the presence of Et_3N, which do not support productive catalytic turnover.

On the basis of the results summarized in Table 1, a catalytic cycle is proposed as shown in Scheme 5. The individual oxidative deformylation steps closely parallel to those observed in the stoichiometric reaction depicted in Scheme 3. In the catalytic cycle, the μ-oxo-dimer **2** reacts with 2-PPA in the presence of O_2 *via* a HAA pathway, producing acetophenone and a formyloxyl radical, along with the formation of a mixed-valence iron intermediate. Control experiments demonstrate that while **2** reacts readily with formic acid, it does not undergo irreversible deactivation in the presence of formate alone. Accordingly, in the presence of Et_3N, the mixed valence iron porphyrin dimer is rapidly regenerated to the μ-oxo-dimer **2** through efficient proton abstraction, thereby preventing

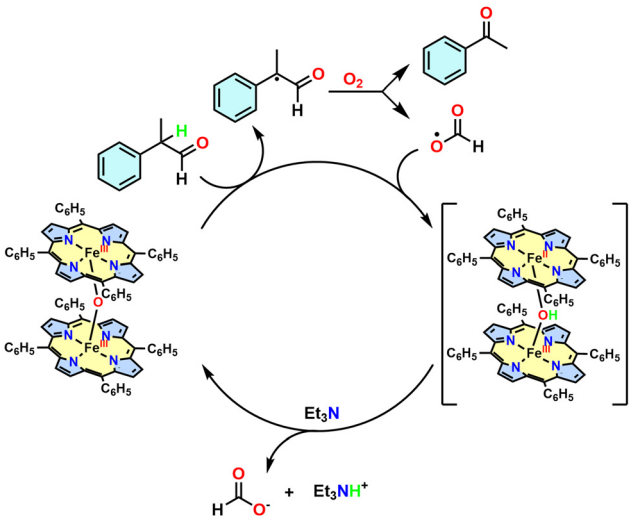

Scheme 5 Proposed catalytic cycle involving [Fe(TPP)]$_2$O (**2**) and 2-PPA in the presence of Et_3N under aerobic conditions.

accumulation of catalytically inactive formate-bound iron(III) species and enabling sustained turnover.

Formation of formate as a reaction product was confirmed by ^1H and ^{13}C NMR spectroscopy in D_2O (Fig. S16 and S17), providing further support for the proposed mechanism. Considering that nucleophilic addition to aldehydes represents an alternative deformylation pathway,[31,39] 2-methyl-2-phenylpropionaldehyde (2-Me-PPA) was employed as a substrate to preclude hydrogen atom abstraction at the α-carbon. Under the optimal catalytic conditions affording the highest turnover with **2** (Table 1, entry 11), no reaction was observed when 2-Me-PPA was used as the substrate, thereby disfavoring nucleophilic attack as the dominant pathway for 2-PPA degradation under the present catalytic conditions.

Conclusions

In this study, the HAA activity of [Fe(TPP)]$_2$O was demonstrated for the first time using the oxidative deformylation of 2-PPA as a model reaction. Spectroscopic and EPR analyses confirmed the generation of a carbon-centered radical intermediate and highlighted the essential role of molecular oxygen in driving C–C bond cleavage and acetophenone formation. Although a direct oxygen-rebound process involving the bridging μ-oxo unit—which could potentially enable a closed catalytic cycle—was not observed, the system nevertheless exhibited strong catalytic performance, achieving a maximum turnover number (TON) of 84 and up to 97% product yield in the presence of the inexpensive base triethylamine. This study presents a green and efficient approach to oxidative deformylation utilizing atmospheric dioxygen as the sole oxidant, without the need for stoichiometric oxidants or external oxygen sources. Notably, μ-oxo-bridged diiron(III) porphyrin complexes are among the most stable and cost-effective porphyrinic species,

readily accessible within porphyrin chemistry. These findings broaden the known reactivity of μ-oxo iron dimers and underscore their potential as tunable catalysts for C–H and C–C bond activations relevant to both biomimetic chemistry and synthetic applications.

Conflicts of interest

The authors declare no conflict of interest.

Data availability

All data supporting this study are included in the supplementary information (SI). Supplementary information: detailed experimental procedures, UV–vis spectra, NMR data, mass spectra, and catalytic reaction data. See DOI: https://doi.org/10.1039/d5dt02565f.

Acknowledgements

Financial support from the National Science and Technology Council (NSTC), Taiwan (Grant NSTC 113-2113-M-001-009 to C.-H. H.) is gratefully acknowledged. We also thank the NMR Laboratory, Mass Spectrometry Laboratory, and Catalysis Center of the Institute of Chemistry, Academia Sinica, for instrumentation and technical support.

References

1 C. Bourdillon, C. Demaille, J. Moiroux and J.-M. Saveant, *J. Am. Chem. Soc.*, 1995, **117**, 11499–11506.
2 M. Newcomb, M. B. Manek and A. G. Glenn, *J. Am. Chem. Soc.*, 1991, **113**, 949–958.
3 K. M. Roberts and J. P. Jones, *Chem. – Eur. J.*, 2010, **16**, 8096–8107.
4 H. Zhao, *RSC Adv.*, 2024, **14**, 25932–25974.
5 S. Jain, F. Ospina and S. C. Hammer, *JACS Au*, 2024, **4**, 2068–2080.
6 S. Shaik, D. Kumar, S. P. de Visser, A. Altun and W. Thiel, *Chem. Rev.*, 2005, **105**, 2279–2328.
7 B. Meunier, S. P. de Visser and S. Shaik, *Chem. Rev.*, 2004, **104**, 3947–3980.
8 H. Li, Y. Zhang, Y. Huang, P. Duan, R. Ge, X. Han and W. Zhang, *Adv. Sci.*, 2023, **10**, 2304605.
9 J. T. Groves, *J. Inorg. Biochem.*, 2006, **100**, 434–447.
10 X. Huang and J. T. Groves, *Chem. Rev.*, 2018, **118**, 2491–2553.
11 N. C. Boaz, S. R. Bell and J. T. Groves, *J. Am. Chem. Soc.*, 2015, **137**, 2875–2885.
12 J. T. Groves and G. A. McClusky, *J. Am. Chem. Soc.*, 1976, **98**, 859–861.
13 M.-J. Kang, W. J. Song, A.-R. Han, Y. S. Choi, H. G. Jang and W. Nam, *J. Org. Chem.*, 2007, **72**, 6301–6304.
14 W. J. Song, Y. J. Sun, S. K. Choi and W. Nam, *Chem. – Eur. J.*, 2006, **12**, 130–137.
15 A. C. Lindhorst, S. Haslinger and F. E. Kühn, *Chem. Commun.*, 2015, **51**, 17193–17212.
16 M. J. Weissenborn and R. M. Koenigs, *ChemCatChem*, 2020, **12**, 2171–2179.
17 F. Jia and Z. Li, *Org. Chem. Front.*, 2014, **1**, 194–214.
18 Y. Kato, T. Yoshino and S. Matsunaga, *ACS Catal.*, 2023, **13**, 4552–4559.
19 T. Guchhait, S. Sasmal, F. S. T. Khan and S. P. Rath, *Coord. Chem. Rev.*, 2017, **337**, 112–144.
20 T. Schuh, O. Kataeva and H.-J. Knölker, *Chem. Sci.*, 2023, **14**, 257–265.
21 M. Balamurugan, E. Suresh and M. Palaniandavar, *RSC Adv.*, 2021, **11**, 21514–21526.
22 R. A. Baglia, J. P. T. Zaragoza and D. P. Goldberg, *Chem. Rev.*, 2017, **117**, 13320–13352.
23 A. J. Jasniewski and L. Que Jr., *Chem. Rev.*, 2018, **118**, 2554–2592.
24 D. M. Kurtz Jr., *Chem. Rev.*, 1990, **90**, 585–606.
25 A. Jozwiuk, A. L. Ingram, D. R. Powell, B. Moubaraki, N. F. Chilton, K. S. Murray and R. P. Houser, *Dalton Trans.*, 2014, **43**, 9740–9753.
26 R.-N. Li and S.-L. Chen, *ChemBioChem*, 2025, **26**, e202400788.
27 U. K. Bagha, J. K. Satpathy, G. Mukherjee, C. V. Sastri and S. P. de Visser, *Org. Biomol. Chem.*, 2021, **19**, 1879–1899.
28 S. H. Bae, X.-X. Li, M. S. Seo, Y.-M. Lee, S. Fukuzumi and W. Nam, *J. Am. Chem. Soc.*, 2019, **141**, 7675–7679.
29 J. Annaraj, Y. Suh, M. S. Seo, S. O. Kim and W. Nam, *Chem. Commun.*, 2005, 4529–4531.
30 J. Cho, S. Jeon, S. A. Wilson, L. V. Liu, E. A. Kang, J. J. Braymer, M. H. Lim, B. Hedman, K. O. Hodgson, J. S. Valentine, E. I. Solomon and W. Nam, *Nature*, 2011, **478**, 502.
31 S. H. Bae, X.-X. Li, M. S. Seo, Y.-M. Lee, S. Fukuzumi and W. Nam, *J. Am. Chem. Soc.*, 2019, **141**, 7675–7679.
32 E. B. Fleischer and T. Srivastava, *J. Am. Chem. Soc.*, 1969, **91**, 2403–2405.
33 F. G. Cantú Reinhard, P. Barman, G. Mukherjee, J. Kumar, D. Kumar, D. Kumar, C. V. Sastri and S. P. de Visser, *J. Am. Chem. Soc.*, 2017, **139**, 18328–18338.
34 Y. J. Jeong, Y. Kang, A.-R. Han, Y.-M. Lee, H. Kotani, S. Fukuzumi and W. Nam, *Angew. Chem., Int. Ed.*, 2008, **47**, 7321–7324.
35 S. R. Bell and J. T. Groves, *J. Am. Chem. Soc.*, 2009, **131**, 9640–9641.
36 M. Guo, T. Corona, K. Ray and W. Nam, *ACS Cent. Sci.*, 2019, **5**, 13–28.
37 S. I. Dikalov and R. P. Mason, *Free Radical Biol. Med.*, 2001, **30**, 187–197.
38 K. M. Kadish, G. Larson, D. Lexa and M. Momenteau, *J. Am. Chem. Soc.*, 1975, **97**, 282–288.
39 W. Zhu, D. Sun, A. Zhou, S. Wang, Y. Zhang, H. P. H. Wong, A. Kumar, X. Lu, P. Wu, S. S. Nag, Y. Wang, K. Ray, S. P. de Visser and W. Nam, *J. Am. Chem. Soc.*, 2025, **147**, 15006–15018.

